

Contents lists available at ScienceDirect

Spectrochimica Acta Part A: Molecular and Biomolecular Spectroscopy

journal homepage: www.journals.elsevier.com/spectrochimica-acta-part-a-molecular-and-biomolecular-spectroscopy





Measurement of chemical penetration in skin using Stimulated Raman scattering microscopy and multivariate curve resolution - alternating least squares

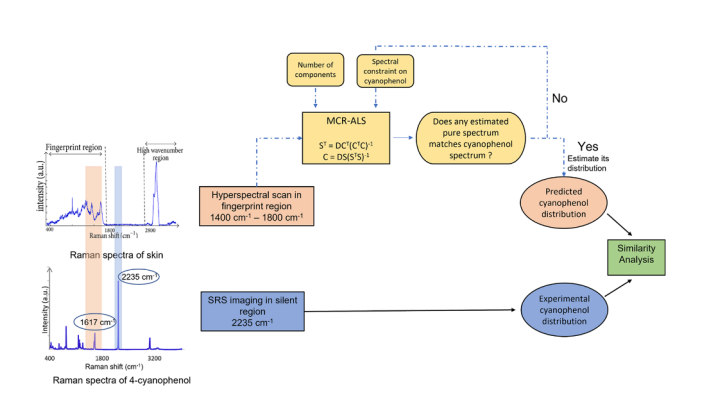
Anukrati Goel ^a, Dimitrios Tsikritsis ^b, Natalie A. Belsey ^{a, b}, Ruth Pendlington ^c, Stephen Glavin ^c, Tao Chen ^{a,*}

- ^a Department of Chemical and Process Engineering, University of Surrey, Guildford, GU2 7XH, UK
- ^b Chemical & Biological Sciences Department, National Physical Laboratory, Hampton Road, Teddington, TW11 0LW, UK
- ^c Unilever Safety & Environmental Assurance Centre, Colworth Science Park, Bedford, MK44 1LQ, UK

HIGHLIGHTS

- Methodology to map distribution of chemicals in skin without using labelling agents.
- Spectral unmixing of hyperspectral Raman imaging data using chemometrics.
- The resolved components provide information on skin physiology.
- Good similarity between predicted and experimental distribution of active ingredient.

GRAPHICAL ABSTRACT



ARTICLE INFO

Keywords: Stimulated Raman Scattering Chemometrics Spectral Unmixing Topical delivery Multivariate analysis

ABSTRACT

The mechanistic understanding of skin penetration underpins the design, efficacy and risk assessment of many high-value products including functional personal care products, topical and transdermal drugs. Stimulated Raman scattering (SRS) microscopy, a label free chemical imaging tool, combines molecular spectroscopy with submicron spatial information to map the distribution of chemicals as they penetrate the skin. However, the quantification of penetration is hampered by significant interference from Raman signals of skin constituents. This study reports a method for disentangling exogeneous contributions and measuring their permeation profile through human skin combining SRS measurements with chemometrics. We investigated the spectral decomposition capability of multivariate curve resolution – alternating least squares (MCR–ALS) using hyperspectral SRS images of skin dosed with 4-cyanophenol. By performing MCR-ALS on the fingerprint region spectral data, the distribution of 4-cyanophenol in skin was estimated in an attempt to quantify the amount permeated at different depths. The reconstructed distribution was compared with the experimental mapping of C=N, a strong

Abbreviations: SRS, Stimulated Raman Scattering; MCR-ALS, Multivariate Curve Resolution Alternating Least Square; LOF, Lack of Fit; SC, Stratum Corneum; SVD, Singular Vector Decomposition.

E-mail address: t.chen@surrey.ac.uk (T. Chen).

^{*} Corresponding author.

vibrational peak in 4-cyanophenol where the skin is spectroscopically silent. The similarity between MCR-ALS resolved and experimental distribution in skin dosed for 4 h was 0.79 which improved to 0.91 for skin dosed for 1 h. The correlation was observed to be lower for deeper layers of skin where SRS signal intensity is low which is an indication of low sensitivity of SRS. This work is the first demonstration, to the best of our knowledge, of combining SRS imaging technique with spectral unmixing methods for direct observation and mapping of the chemical penetration and distribution in biological tissues.

1. Introduction

Skin is a complex multi-layered tissue with stratum corneum (SC) being the superficial layer providing a barrier against exogenous materials, such as the ingredients in pharmaceutical, cosmetic, and other chemical products. Monitoring the penetration and distribution of the ingredients is important to assess its efficacy and/or safety for various applications [1]. The commonly used in vitro/ex vivo techniques to assess skin permeation such as diffusion cell coupled with chromatographic methods [2], tape stripping [3] and fluorescent imaging [4] either do not elucidate the lateral spatial distribution of chemicals within skin layers or are dependent on the use of fluorescent probes, which perturb the uptake of small molecules. To this end Raman spectroscopy has been shown to be a powerful technique for chemical imaging without the use of exogenous labels [5-7]. The Raman effect is based on inelastic light scattering which occurs due to a change in the vibrational or rotational levels of molecules upon interacting with light. Since the vibrational modes are intrinsic to a molecule, its chemical information can be deduced which makes Raman spectroscopy a chemically sensitive analytical technique [8]. Raman microscopy has been successfully applied both in vitro and in vivo to track permeation of various active ingredients, penetration enhancers and excipients [9-14]. It has also been employed to analyse skin physiology and diagnosis of pathological states [15-19].

Although very powerful for chemical characterization, spontaneous Raman spectroscopy is unable to provide fast high-resolution imaging due to inefficiency of the Raman scattering process [20]. Stimulated Raman scattering (SRS) microscopy, an advanced Raman imaging technique, overcomes this challenge and offers up to video-rate Raman imaging with submicron spatial resolution [21-23]. In SRS, the molecular vibrations are stimulated by the interference between two optical beams, the pump and the Stokes. When the frequency difference Ω between these two beams is tuned to match a molecular vibration of interest ($\Omega = \omega_p - \omega_s$), a coherent Raman excitation occurs. This boosts scattering by multiple orders of magnitude compared to spontaneous Raman spectroscopy, allowing imaging up to video-rate speed [24]. SRS imaging uses a modulation transfer scheme to detect the transfer of energy between the two beams which is usually measured either as a loss in the pump beam (stimulated Raman loss, SRL) or a gain in the Stokes beam (stimulated Raman gain, SRG) and offers the advantage that the Raman signal detection is unaffected by emitted fluorescence. Moreover, a linear correlation between the SRS signal intensity and molecular concentration (within the same optical plane) facilitates a direct concentration analysis of the sample, forging SRS microscopy as a robust and quantitative chemical imaging method.

The ability to identify skin physiology and track distribution of molecules within skin layers without the use of labelling makes SRS a powerful technique to assess dermal delivery of topical chemicals [25–27]. The excellent imaging ability of SRS in skin research was first demonstrated by Saar *et al.* in 2011 where they observed the permeation of ketoprofen and ibuprofen solubilized in deuterated propylene glycol [28]. The group also compared the relative importance of hair follicular and intercellular pathways in drug penetration in mouse skin. Another research by Belsey *et al.* observed both drug deposition and crystallization of drug within porcine skin simultaneously after application of a close-to-saturation solution of ibuprofen in propylene glycol-d8 solvent [29]. Most recently, Feizpour *et al.* performed depth and time resolved

SRS imaging of an anti-inflammatory drug in mouse skin and leveraged convolutional neural network to identify various domains of the tissue and quantify the relative uptake of drug in the SC [30].

Although SRS microscopy can be used for most molecules of interest, the acquired signals contain contributions from various endogenous chemical species in the sample. Such superimposed Raman signals manifest challenges in single frequency SRS imaging. This can be overcome by integrating hyperspectral imaging (analysing over a range of frequencies) with spectral unmixing methods to disentangle the contribution of ingredients of interest from overlapping endogenous signals [31,32]. Of particular interest is the method of multivariate curve resolution - alternating least square (MCR-ALS) [33-35]. MCR-ALS has been successfully applied to process hyperspectral data for a wide range of applications in process analysis [36], analytical chemistry [37], pharmaceutical quality control [38], remote sensing [33], cellular biological systems [39-41], direct quantification of falsified drugs [42], etc. For skin analysis, Schleusener et al. used MCR-ALS to identify different skin components in skin sections containing hair follicles [43]. Most recently, Choe et al. applied MCR-ALS to determine water concentration profiles in the stratum corneum [44]. The ability of MCR-ALS to resolve spectral contribution of a chemical in skin was recently demonstrated by Stella et al. where they used it to investigate the diffusion profile of Delipidol in upper layers of human reconstructed skin from confocal Raman spectroscopy data [45]. Although the study predicted the penetration profile of the active ingredient in the skin cross section, it did not offer a method to verify whether the predicted concentration matched with the experimental distribution.

In this study we retrieved the distribution of 4-cyanophenol in skin by applying MCR-ALS to an SRS hyperspectral stack acquired across the fingerprint spectral region, despite the interference from strong signals in skin tissue. The reconstructed 4-cyanophenol distribution was compared with the experimental mapping within the skin to validate the reliability of spectral unmixing by MCR-ALS. To obtain the experimental distribution, C\(\exists N\), a strong stretching vibration present in 4-cyanophenol, was targeted by SRS imaging as this vibrational band is located in the biological silent region, which exhibits no signal from skin tissue. Since the skin is spectroscopically 'silent' at this vibration mode, the signals at C=N vibration maps true distribution of 4-cyanophenol and can be directly compared to assess if the distributions from both the experimental and computational methods are consistent. Furthermore, a validation study of the MCR-ALS algorithm was carried out to demonstrate that the resolved distribution mapping is proportional to the concentration of the sample.

Through this research, we present a proof of concept on the reliability of MCR-ALS to isolate the Raman signals of active ingredients from endogenous species. Furthermore, we reported the first use of MCR-ALS to retrieve the diffusion profile of chemicals in skin from hyperspectral SRS images. The methodology is a novel contribution in the context of skin permeation for identifying distribution of ingredients within skin layers.

2. Materials & methods

2.1. Specimen preparation

For the validation of MCR-ALS, different concentrations of 4-cyanophenol (Sigma Aldrich, UK) solution, specifically $100~{\rm mg~mL^{-1}}$, $50~{\rm mg}$

 $\rm mL^{-1},\,20~mg~mL^{-1}$ and 0 mg $\rm mL^{-1}$ were prepared in equi-volume solution of propylene glycol (MP Biomedicals, UK) and ultrapure water (termed hereafter as propylene glycol solution). A droplet of all the four samples were sealed between two glass coverslips (#1.5, Menzel Glasser) and imaged with the SRS microscope immediately.

2.2. Preparation of skin samples

Human abdominal skin was purchased from ALPHENYX (France) and was stored at $-20~^\circ\text{C}$ until use. The skin was obtained from a 40-year-old female from abdominal plastic surgery. 70 mg mL $^{-1}$ 4-cyanophenol solution was topically applied onto the full thickness skin for 4 h at a temperature of 32 $^\circ\text{C}$. After the diffusion period, the dosed skin sample was frozen at $-20~^\circ\text{C}$ and sectioned vertically using a cryomicrotome (Leica CM 1850) to obtain 30 μm thick cross-sections. An untreated skin cross-section (control) of same thickness was also obtained using the same procedure. The samples were mounted on glass coverslips (#1.5, Menzel Glasser) and imaged as described below.

2.3. SRS imaging

SRS images were acquired on a Leica SP8 laser scanning microscope coupled to a PicoEmerald-S laser system. The PicoEmerald-S outputs two pulsed 2 ps laser beams: a 1031.2 nm Stokes beam which was spatially and temporally overlapped with a tuneable pump beam. The Stokes beam was modulated at 20 MHz and SRL signals were detected using a silicon-based detector and lock-in amplifier (UHFLI, Zurich instruments). Images were acquired with a water immersion \times 40 magnification lens (1.1NA, Leica) used in conjunction with an oil immersion condenser lens (1.4NA, Leica). The laser power was set to 30 % which corresponds to approximately 10 mW for the pump beam and 30 mW for the Stokes beam at the sample.

For validation experiments, a hyperspectral scan from 877.4 nm to 901.1 nm with a step size of 0.1 nm was performed for each sample of four different concentrations resulting in raster images at 239 spectral

points. A stack of 64 * 64 pixel images with a pixel area of 7.28 * 7.28 μm^2 for each sample was acquired generating four XY- Ω stacks of 239 images each. Here, X and Y represent the number of pixels in \times and y direction and Ω is the wavenumber encompassing the hyperspectral scan which results to give a data cube of 64 * 64 * 239 for each sample. The corresponding scan covering 1400 – 1700 cm $^{-1}$ was acquired as it includes the Raman peaks from both 4-cyanophenol and propylene glycol (Supplementary Fig. S1). Further image processing details are given in section 2.4. In addition to the use of consistent instrument and image acquisition parameters, image processing steps have also been consistently applied across the four samples.

The SRS hyperspectral images of the skin samples were generated by tuning the pump laser wavelength from 869.7 nm to 901.1 with increments of 0.2 nm. This resulted in XY-Ω stacks of 158 images of 64 * 64 pixels each where Ω is the Raman shift ranging from 1400 -1800 cm⁻¹. The total acquisition time for the hyperspectral scan is 27 min. Although the time taken to acquire a single image is around 2 s, majority of the time is taken up to tune the microscope to the given wavenumbers. In addition to the hyperspectral scan, a 512 * 512 pixel SRS image of the skin was acquired at 2235 cm⁻¹ to map the signal distribution of 4-cyanophenol at the C\(\equiv N\) vibrational mode. This peak was confirmed from hyperspectral SRS data in the silent region as shown in Supplementary Fig. S2. The pixel dwell time of this scan was limited to 7 μs covering a pixel area of 0.91 * 0.91 μm². Please note that an offresonance signal (where neither skin nor any exogenous species is Raman active) at 2257 cm⁻¹ is subtracted from all the measurements of the resonant peak at 2235 cm⁻¹.

2.4. Data analysis

The underlying assumption behind MCR-ALS is the additive bilinear relationship between different constituents of a mixture such that the raw spectra matrix D (n^*m) can be decomposed into its pure concentration profile C (n^*k) and pure spectral profiles S (m^*k) for k species in the mixture [46]. D (n^*m) represents the dimension of the raw data

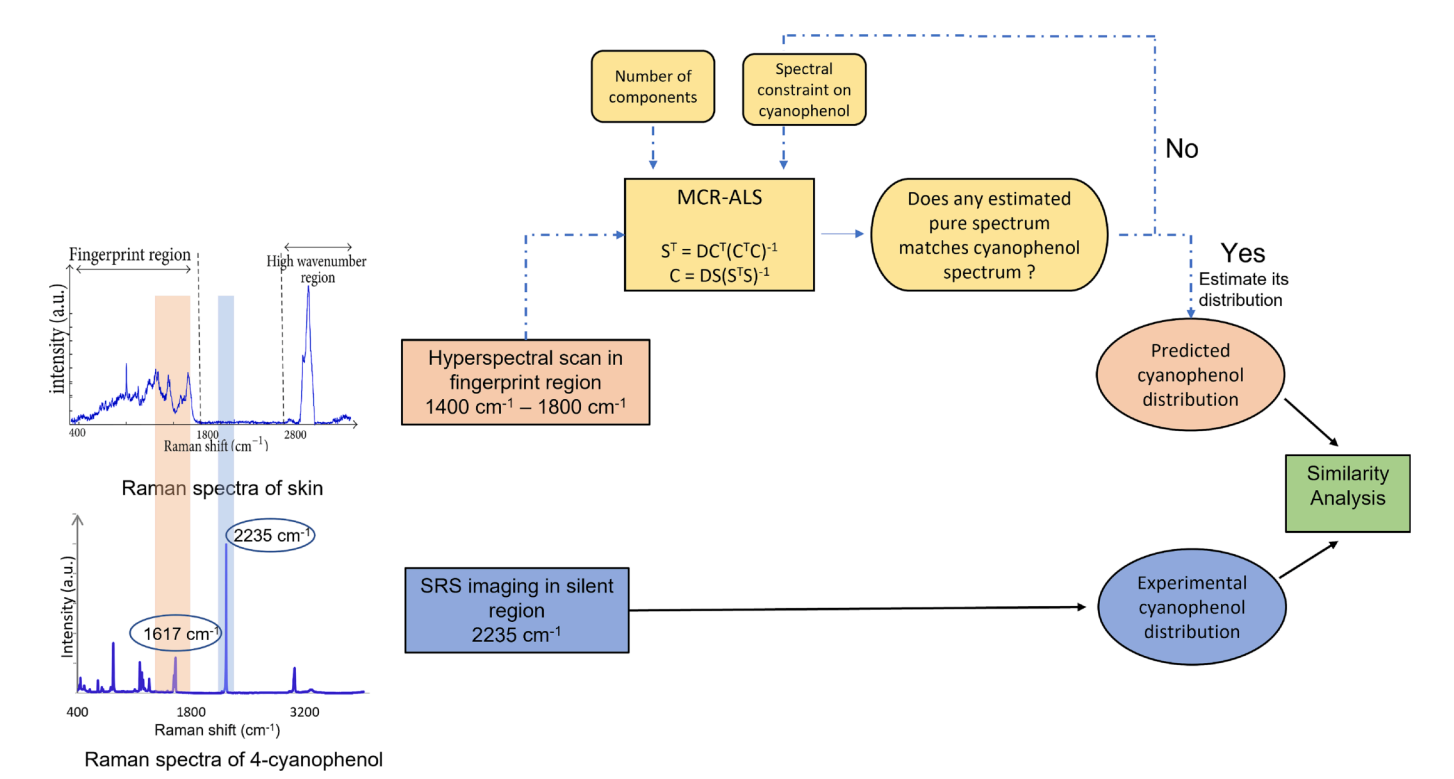


Fig. 1. Framework of MCR-ALS analysis to identify distribution of 4-cyanophenol in skin. The framework identifies the spectral range to be evaluated, process the hyperspectral scan with MCR-ALS and compare it with experimental data in the 'silent' region.

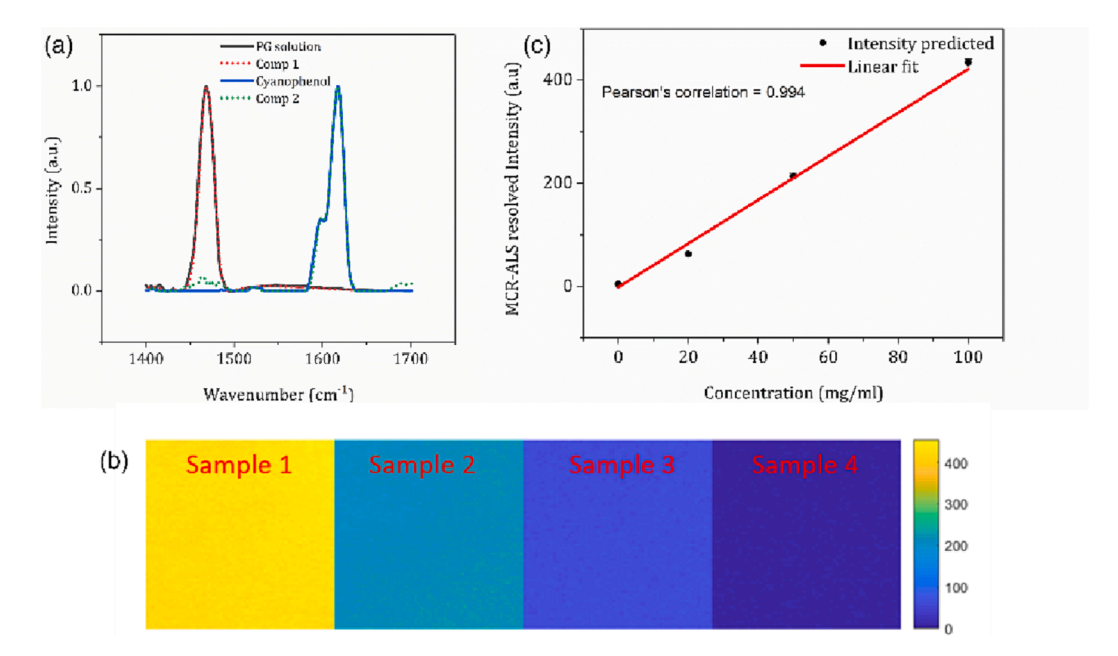


Fig. 2. MCR-ALS analysis of 4-cyanophenol solutions with known concentration (100/50/20/0 mg mL⁻¹ for samples 1–4). (a) Resolved spectra of component 1 (red) and component 2 (green) identifying with the spectrum of propylene glycol solution (black) and 4-cyanophenol (blue) obtained from confocal Raman spectroscopy (b) MCR-ALS resolved 2-D 4-cyanophenol distribution (64 * 64 pixels) of the samples of known concentrations. (c) MCR-ALS resolved average intensity show linear relationship with known 4-cyanophenol concentration. (For interpretation of the references to colour in this figure legend, the reader is referred to the web version of this article.)

matrix acquired at n spatial locations and m spectral points. Mathematically,

$$D = CS^T + E \tag{1}$$

where $E\left(n^{*}m\right)$ is the residual error unexplained by the resolved components.

The number of species k is determined either by different mathematical approaches or based on prior knowledge of the system [47]. The reliability of decomposition can be estimated by evaluating the lack of fit (LOF). This is defined as the difference between input spectra \boldsymbol{D} and the data reproduced from \boldsymbol{CS}^T resolved using MCR-ALS. It can be estimated by the expression:

LOF =
$$100*\sqrt{\frac{\sum \left(d_{ij} - d_{ij}^*\right)^2}{\sum d_{ij}^2}}$$
 (2)

where d_{ij} and d_{ij}^* are matrix elements of input matrix D and reproduced matrix CS^T respectively.

Firstly, the MCR-ALS method was used to analyse the hyperspectral SRS data of the four 4-cyanophenol solution samples described in Section 2.1, for the purpose of method validation with known concentrations. The hyperspectral SRS stacks were imported to ImageJ [48] and an 8-bit gray value at each pixel was extracted. The hyperspectral scans of the four 4-cyanophenol solution samples were unfolded to form a validation spectral matrix D, where each row represents spectra at each pixel. The validation dataset was decomposed using MCR-ALS into two components. Non negativity constraint was imposed on concentration values and a 0.01 % convergence criterion was used. The MCR-ALS analysis in this study was performed using the MCR-ALS program [49] on Matlab R2020b. The rows in the obtained spectral matrix S represent the spectrum of each component while the resulting concentration matrix C was refolded back (known as 'reconstructed' distribution) to generate a concentration map of each component for all the four samples of varying concentration. The MCR-ALS resolved 4-cyanophenol concentration map for each of the four samples was pixel-averaged and correlated with the nominal 4-cyanophenol concentration in the sample.

Subsequently, the MCR-ALS analysis of skin samples was carried out in the same manner described above, but in addition, it required determining the number of components which were not as straightforward as for the case above. The number of components (i.e. chemical species) contributing to spectral dataset D of skin sample was determined by Singular Value Decomposition (SVD) [50]. In SVD, the relevance of each component is determined by the value of the eigen value where higher eigen value is related to more biochemical contribution. In addition to SVD, the number of components were optimized by manually inspecting the decomposed spectra for different number of components ($k = \{3,6\}$). Once the number of components for control sample was determined, the treated sample was analysed using one additional component for 4-cyanophenol. With the determined number of contributing species and an initial estimate in spectra, C and S were calculated and optimized iteratively using equation (1) until convergence within 0.01 % was reached. The MCR-ALS decomposition was constrained to produce non-negative spectral and concentration profile to obtain physically relevant results. The MCR-ALS workflow followed in this work is shown in Fig. 1. An important point to note here is that the resolved chemical components in MCR-ALS analysis do not necessarily correspond to 4-cyanophenol. It is a common practice in MCR-ALS analysis to use spectral equality constraint to guide the algorithm to obtain the concentration map of a target species. An equality constraint on a spectrum fixes the spectrum of target species to its known profile determined from confocal Raman spectroscopy data. The Confocal Raman spectroscopy setup to obtain the Raman profile of chemicals is discussed in supplementary information. In the event the algorithm seemed ineffective to identify 4-cyanophenol as a component, the analysis was rerun by constraining a component with the reference spectrum of 4-cyanophenol to help the algorithm to estimate its concentration in skin (see workflow in Fig. 1). The quality of the data resolution was assessed using LOF as estimated from equation (2).

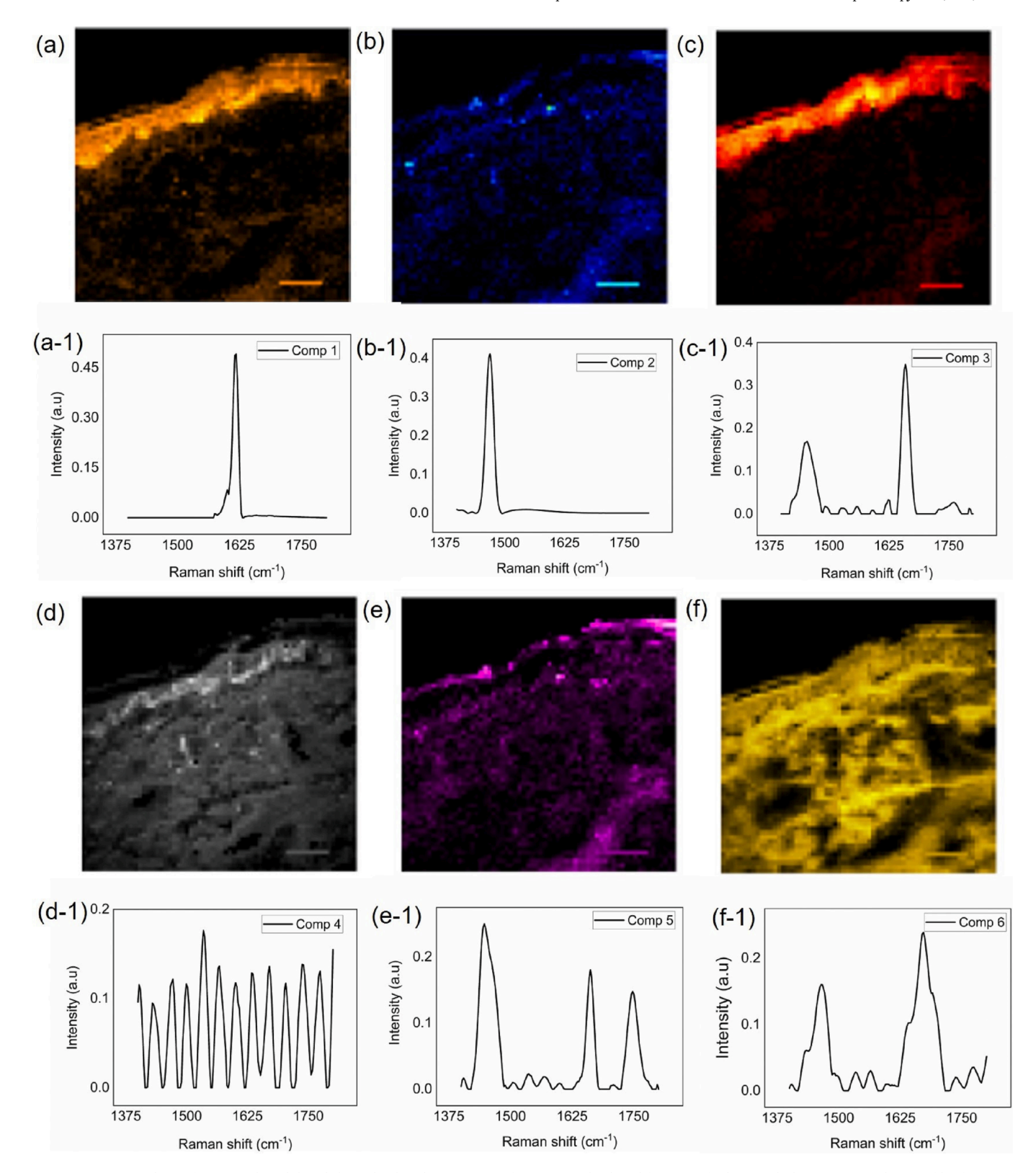


Fig. 3. MCR-ALS analysis of 4-cyanophenol dosed skin. The distribution maps of six species displayed from (a)-(f) along with their corresponding profiles from (a-1) to (f-1). The scale bar in the images is set to 73 μm.

3. Results & discussion

3.1. Validation of MCR-ALS

To validate the reliability of MCR-ALS in mapping the concentration

of the 4-cyanophenol within the sample, hyperspectral SRL imaging of 4-cyanophenol solutions of varying strength to retrieve its concentration was performed. The decomposed spectra of two components are in good accordance with the spontaneous Raman spectrum of 4-cyanophenol and propylene glycol solution (Fig. 2(a) solid lines). The MCR-ALS

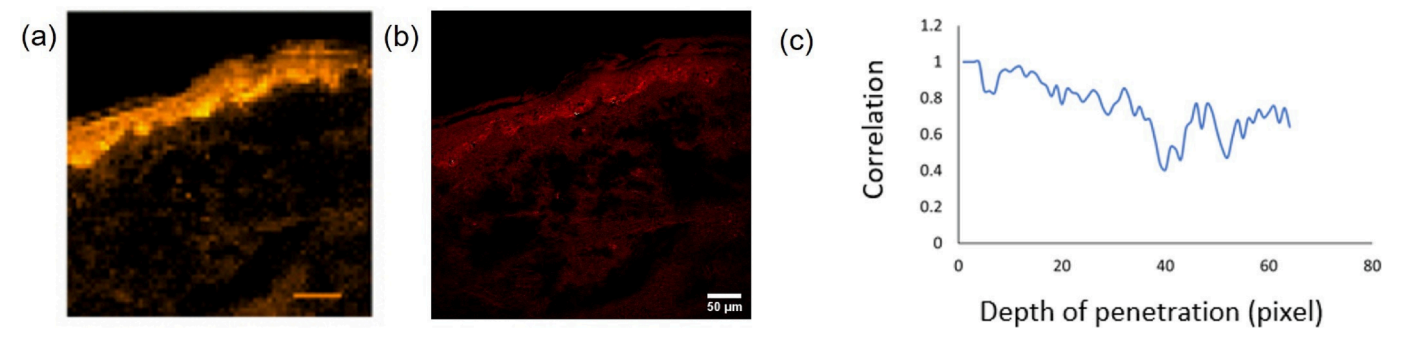


Fig. 4. (a) Distribution profile of the first component corresponding to 4-cyanophenol from MCR-ALS analysis. The scale bar in the image is set to 73 μm. (b) SRS imaging of dosed sample at 2235 cm¹. (c) Correlation between reconstructed and experimental 4-cyanophenol distribution of skin dosed for 4 h.

resolved distribution map corresponding to 4-cyanophenol across the samples displayed in Fig. 2(b) follows a linear response between the resolved average intensity and sample concentration of 4-cyanophenol with a Pearson correlation of 0.994 (Fig. 2(c)). This establishes the proportionality between resolved intensity of chemical species and their concentration in the sample.

3.2. Analysing 4-cyanophenol penetration in skin

The capability of MCR-ALS to map the permeation of a chemical in skin was investigated by topical treatment of skin with a 4-cyanophenol formulation in propylene glycol. A spectral range from 1400 to 1800 cm⁻¹ was analysed, where 4-cyanophenol has a strong Raman mode at $\sim 1617~{\rm cm}^{-1}$ but is overlapped with the Raman bands of various skin components (refer to Fig. 1). Thus, a single frequency SRS imaging at 1617 cm⁻¹ cannot accurately map the target molecule because the contrast of the image also contains endogenous skin components. To carry out MCR-ALS analysis of hyperspectral data, firstly SVD was implemented to determine the major chemical components in the control system which were identified to be five based on the magnitude of eigen values and manual inspection. With six components for the treated system and using only the non-negativity constraint on spectra and concentration, the algorithm did not identify 4-cyanophenol as a chemical species in the system (Supplementary Fig. S3) as none of the components' spectrum profile matched with the 4-cyanophenol spectrum. In order to obtain the distribution map of 4-cyanophenol within skin, a spectral equality on 4-cyanophenol was applied in addition to non-negativity constraint and MCR-ALS analysis was repeated using six components. The analysis decomposed raw data into concentration maps of six species (Fig. 3(a) - 3(f)) and their corresponding spectral profiles (Fig. 3(a-1) - 3(f-1)) using additional spectral equality constraint on 4-cyanphenol. The LOF for the analysis was found to be 6.24 %.

The distribution of 4-cyanophenol within skin layers can be estimated from the concentration map of the first component Fig. 3(a) as its spectral profile was constrained with the reference spectrum of 4-cyanophenol obtained from confocal Raman spectroscopy. To assess if the prediction correctly identifies the 4-cyanophenol distribution, SRS imaging for C \equiv N was also performed. This strong vibrational mode in 4-cyanophenol occurs in the biological 'silent' region of the Raman spectrum, without interference from skin tissue components. The average 2D Pearson's correlation in relation with pixel intensities between reconstructed (Fig. 4(a)) and experimental mapping (Fig. 4(b)) using equation (3) was calculated to be 0.79.

$$\frac{\sum_{m}\sum_{n}(A_{mn}-\overline{A})(B_{mn}-\overline{B})}{\sqrt{\left(\sum_{m}\sum_{n}(A_{mn}-\overline{A})^{2}\right)}\sqrt{\left(\sum_{m}\sum_{n}(B_{mn}-\overline{B})^{2}\right)}}$$
(3)

To investigate further, the correlation was plotted as a function of penetration depth (roughly defined as the y axis of the image hereafter) as shown in Fig. 4(c). It can be observed that the correlation is higher in the upper layers of skin, and it decreases with penetration depth as the concentration of 4-cyanophenol in deeper layers decreases.

To explore further, the MCR-ALS analysis was carried out to predict the distribution of 4-cyanophenol in skin dosed for 1-hour using the same protocol followed for skin dosed for 4 h. The average correlation between reconstructed (Fig. 5(a)) and experimental (Fig. 5(b)) 4-cyanophenol distribution for 1- hour dosed skin was observed to be 0.91.

The reason for higher correlation for 1-hour dosed skin could be because of the less presence of weaker SRS signals in the skin. As the dosing time was low, the chemical could not penetrate to the deeper skin layers and most of the 4-cyanophenol was distributed in the upper layers resulting in stronger signal intensity and thus the algorithm was able to resolve the data better. In contrast, 4-cyanophenol penetrated the

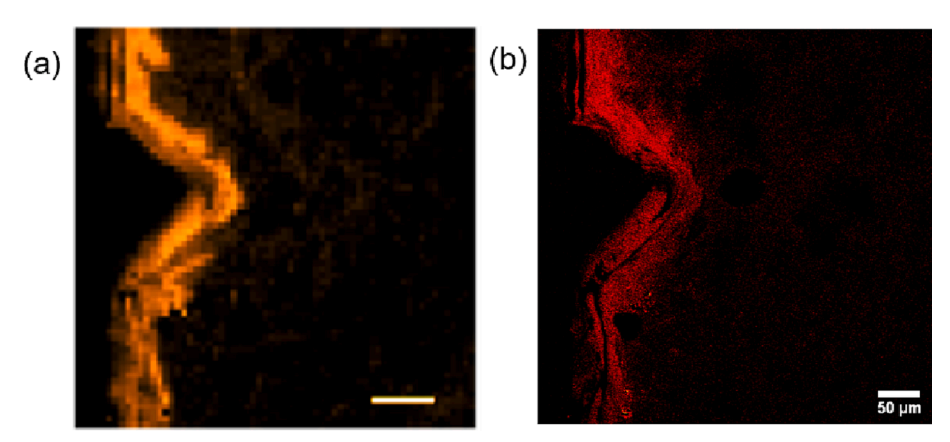


Fig. 5. (a) MCR-ALS reconstructed and (b) Experimental distribution of 4-cyanophenol in skin dosed for 1-hour. The scale bar in the image (a) is set to 73 µm.

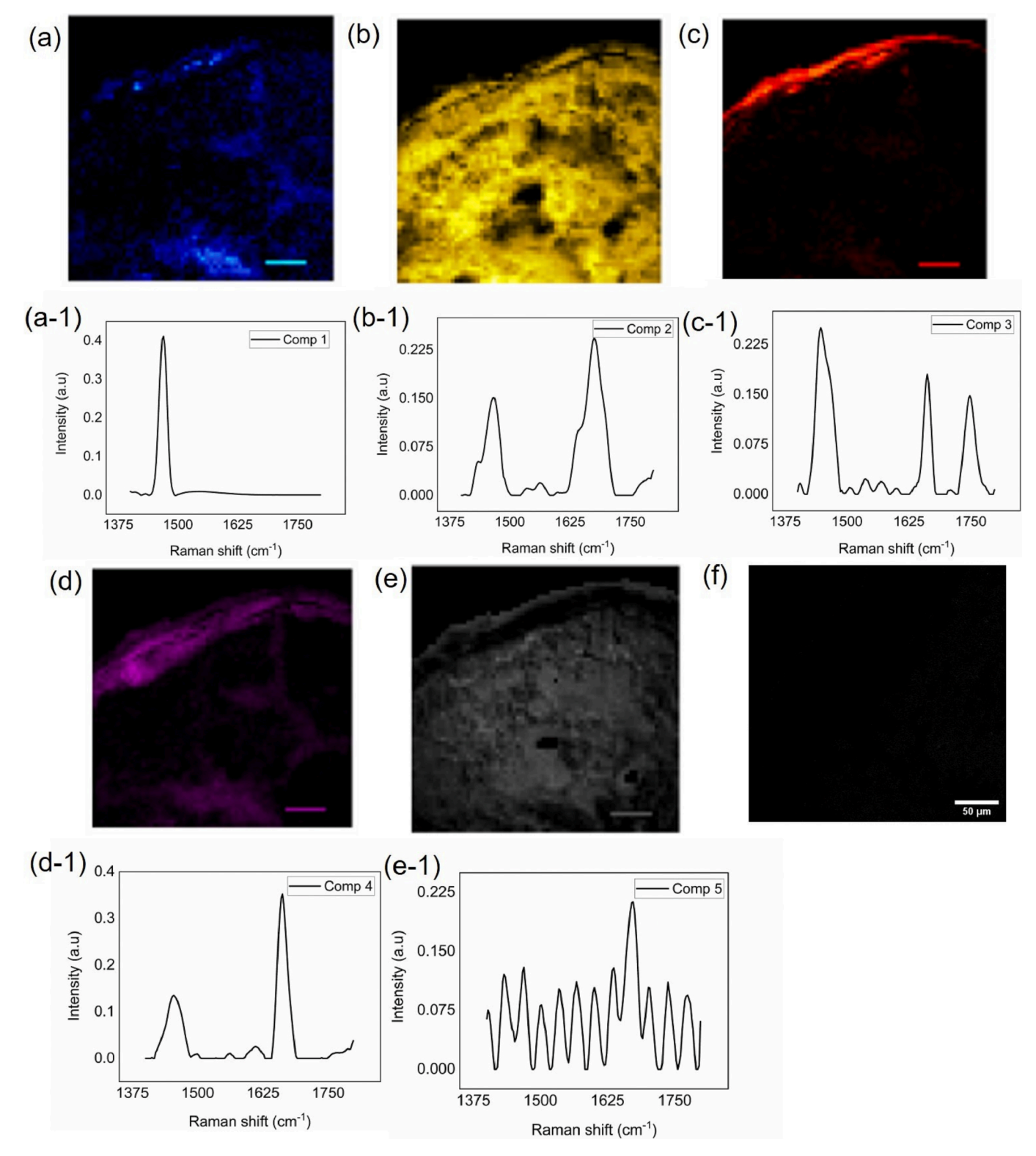


Fig. 6. MCR-ALS analysis of untreated skin/control. (a)-(e) The distribution maps of identified five components with the corresponding spectral profile (a-1) – (e-1). (f) SRS imaging at 2235 cm⁻¹ indicating no presence of 4-cyanophenol in control. The scale bar in the images (a)-(e) is set to 73 μm.

deeper layers of skin when it was dosed for longer times. Since the concentration at deeper layers is low, SRS signal was low or possibly the concentration was below the detection limit of SRS. This indicates the limitation of SRS due to its low chemical sensitivity [51–53]. Nonetheless, the algorithm was able to resolve the distribution of 4-cyanophenol from overwhelming skin signals despite the hyperspectral data having eight times less spatial resolution than the experimental data acquired in

silent region.

The components resolved using MCR-ALS can be observed in Fig. 3, where the 4-cyanophenol penetrated the lower layers of skin although a major amount of chemical was distributed in the epidermis, while most of the propylene glycol penetrated to the deeper layers of tissue as can be seen from the mapping of the second chemical component. To identify the remaining components in the analysis, an MCR-ALS analysis of the

Table 1A percentage spectral matching of resolved dosed components with resolved components of control and 4-cyanophenol. The components sharing a maximum similarity with the chemical species are highlighted in bold.

	4-Cyanophenol	Control Comp1	Control Comp2	Control Comp3	Control Comp4	Control Comp5
Comp1	100	7	14	16	5	17
Comp2	7	100	34	41	19	13
Comp3	6	23	56	39	95	40
Comp4	18	10	0.34	5	1	70
Comp5	1	41	36	99	42	28
Comp6	5	24	99	43	70	41

untreated skin (control) was carried out using five components, constraining them to be non-negative. The decomposed raw data into concentration map and spectra is shown in Fig. 6. Component 2 has a peak at $\sim 1677 \text{ cm}^{-1}$ which can be attributed to the amide I beta sheet vibrational mode, while component 3 has a peak at ~ 1658 cm⁻¹ consistent with C=O amide I alpha helix proteins which are predominantly confined to the SC, and a peak at $\sim 1750~\text{cm}^{-1}$ which is assigned to C=O vibrations in lipids and phospholipids [54-56]. An amide II peak at $\sim 1450~{\rm cm}^{-1}$ in component 4 can be assigned to the C—H vibration in lipids and proteins. The LOF for MCR-ALS analysis of the control sample was assessed to be 3.94 %. The identified species in the control except for component 5 represent different skin layers apart from component 1 which represents the profiling of propylene glycol. The chemical entities identified in untreated skin can be compared with the remaining components in the treated skin which can be attributed to different skin layers.

To investigate the similarity of resolved components from MCR-ALS analysis of dosed skin with the spectra of chemicals, a spectral percentage matching based on Euclidean distance is presented in Table 1. The components sharing a maximum similarity with the chemical species are highlighted in bold.

As can be inferred from reference matching, the first component matches with the 4-cyanophenol spectrum as it was constrained while the second component compares well with propylene glycol. Component 3, 5 and 6 identifies with the resolved components from the undosed skin control which can be attributed to different skin components and represent different skin layers. In this work, applying a spectral equality constraint on the ingredient of interest ensured its profiling of diffusion kinetics within skin layers. The analysis not only resolved the distribution of the active ingredient in skin tissue despite its overwhelming signals, but also provided information on the skin physiology.

4. Conclusions

The study explored the capability of MCR-ALS to disentangle the distribution of different chemical species from a region of overlapping Raman bands based on SRS hyperspectral imaging. Such convoluted signals manifest challenges in single frequency imaging due to a lack of specific chemical contrast. Coupling hyperspectral imaging with MCR-ALS analysis provides a unique approach to resolve the inherent complexity of skin tissue. The method was first validated with 4-cyanophenol solution in propylene glycol and was found to be specific and linear. The method was then applied to hyperspectral SRS stack of skin topically treated with 4-cyanophenol solution. Applying a spectral equality constraint ensured profiling of 4-cyanophenol and the excipient. The resolved mapping of 4-cyanophenol was compared with the SRS imaging at the C=N stretching vibration, a strong Raman band in 4cyanophenol and occurs within the 'silent' region where skin has no signal interference. Good similarity between MCR-ALS resolved and experimental distribution was observed which could be improved by enhancing the sensitivity of SRS. Nonetheless, the study confirms the reliability of MCR-ALS to isolate the signals of a target molecule from its complex biological environment. The other components were identified

to be comprising of skin constituents from various skin layers as resolved by the MCR-ALS analysis of untreated skin. The ability of MCR-ALS to resolve the signals of active ingredients in SRS imaging can pave the way for a label free imaging without the use of deuterium or alkyne tags [57]. Overall, these results present a proof of concept to map the distribution of chemicals within skin layers by utilizing chemometrics to disentangle the superimposed signals in hyperspectral Raman dataset.

CRediT authorship contribution statement

Anukrati Goel: Investigation, Formal analysis, Methodology, Writing – original draft. Dimitrios Tsikritsis: Investigation, Writing – review & editing. Natalie A. Belsey: Conceptualization, Writing – review & editing, Supervision, Funding acquisition. Ruth Pendlington: Supervision, Validation, Writing – review & editing. Stephen Glavin: Supervision, Validation, Writing – review & editing. Tao Chen: Conceptualization, Writing – review & editing, Supervision, Funding acquisition.

Declaration of Competing Interest

The authors declare that they have no known competing financial interests or personal relationships that could have appeared to influence the work reported in this paper.

Data availability

Data will be made available on request.

Acknowledgements

This work was funded by the National Centre for the Replacement, Refinement and Reduction of Animals in Research, UK (NC3Rs, grant number NC/T001720/1) and Unilever, UK. It was also part-funded by the UK Department of Business, Energy and Industrial Strategy through the National Measurement System programme. This work was also supported by the Community for Analytical Measurement Science through a 2020 CAMS Fellowship Award to Natalie Belsey funded by the Analytical Chemistry Trust Fund.

Appendix A. Supplementary material

Supplementary data to this article can be found online at https://doi.org/10.1016/j.saa.2023.122639.

References

- V.R. Leite-Silva, et al., Delivery of drugs applied topically to the skin, Expert. Rev. Dermatol. 7 (4) (2012) 383–397.
- [2] L. Bartosova, J. Bajgar, Transdermal drug delivery in vitro using diffusion cells, Curr. Med. Chem. 19 (27) (2012) 4671–4677.
- [3] A.V. Rawlings, P.J. Matts, Stratum corneum moisturization at the molecular level: an update in relation to the dry skin cycle, J, Invest. Dermatol. 124 (6) (2005) 1099–1110.
- [4] J. Veiro, P. Cummins, Imaging of skin epidermis from various origins using confocal laser scanning microscopy, Dermatology 189 (1) (1994) 16–22.
- [5] C. Krafft, J. Popp, The many facets of Raman spectroscopy for biomedical analysis, Anal. Bioanal. Chem. 407 (3) (2015) 699–717.
- [6] D. Kurouski, et al., Infrared and Raman chemical imaging and spectroscopy at the nanoscale, Chem. Soc. Rev. 49 (11) (2020) 3315–3347.
- [7] A. Gowen, et al., Recent applications of chemical imaging to pharmaceutical process monitoring and quality control, Eur. J. Pharm. Biopharm. 69 (1) (2008) 10–22.
- [8] S. Tfaili, et al., Confocal Raman microspectroscopy for skin characterization: a comparative study between human skin and pig skin, Analyst 137 (16) (2012) 3673–3682.
- [9] L. Franzen, et al., Towards drug quantification in human skin with confocal Raman microscopy, Eur. J. Pharm. Biopharm. 84 (2) (2013) 437–444.
- [10] P.J. Caspers, et al., In vivo confocal Raman microspectroscopy of the skin: noninvasive determination of molecular concentration profiles, J, Invest. Dermatol. 116 (3) (2001) 434–442.

- [11] L. Franzen, J. Anderski, M. Windbergs, Quantitative detection of caffeine in human skin by confocal Raman spectroscopy–A systematic in vitro validation study, Eur. J. Pharm. Biopharm. 95 (2015) 110-116.
- [12] S.M. Ascencio, et al., Confocal Raman microscopy and multivariate statistical analysis for determination of different penetration abilities of caffeine and propylene glycol applied simultaneously in a mixture on porcine skin ex vivo, Eur. J. Pharm. Biopharm. 104 (2016) 51–58.
- [13] N. Jung, et al., Application of confocal raman microscopy for the characterization of topical semisolid formulations and their penetration into human skin Ex Vivo, Pharm. Res. 39 (5) (2022) 935–948.
- [14] R. Krombholz, Y. Liu, D.J. Lunter, In-line and off-line monitoring of skin penetration profiles using confocal raman spectroscopy, Pharmaceutics 13 (1) 2021) 67.
- [15] L. Franzen, M. Windbergs, Applications of Raman spectroscopy in skin research—from skin physiology and diagnosis up to risk assessment and dermal drug delivery, Adv. Drug Deliv. Rev. 89 (2015) 91-104.
- [16] C. Kallaway, et al., Advances in the clinical application of Raman spectroscopy for cancer diagnostics, Photodiagn. Photodyn. Ther. 10 (3) (2013) 207-219.
- A. Nijssen, et al., Discriminating basal cell carcinoma from perilesional skin using high wave-number Raman spectroscopy, J. Biomed. Opt. 12 (3) (2007), 034004.
- [18] I.P. Santos, et al., Improving clinical diagnosis of early-stage cutaneous melanoma based on Raman spectroscopy, Br. J. Cancer 119 (11) (2018) 1339-1346.
- Y. Liu, D.J. Lunter, Selective and sensitive spectral signals on confocal Raman spectroscopy for detection of ex vivo skin lipid properties, Translational Biophotonics 2 (3) (2020).
- [20] R.R. Jones, et al., Raman techniques: fundamentals and frontiers, Nanoscale Res. Lett. 14 (1) (2019) 1-34.
- [21] W.J. Tipping, et al., Stimulated Raman scattering microscopy: an emerging tool for drug discovery, Chem. Soc. Rev. 45 (8) (2016) 2075-2089.
- [22] D. Zhang, et al., Fast vibrational imaging of single cells and tissues by stimulated Raman scattering microscopy, Acc. Chem. Res. 47 (8) (2014) 2282–2290.
- [23] D. Fu, Quantitative chemical imaging with stimulated Raman scattering microscopy, Curr. Opin. Chem. Biol. 39 (2017) 24-31.
- [24] B.G. Saar, et al., Video-rate molecular imaging in vivo with stimulated Raman scattering, Science 330 (6009) (2010) 1368-1370.
- [25] C.W. Freudiger, et al., Stimulated Raman scattering microscopy for label-free chemical imaging, Opt. Photonics News 20 (12) (2009) 30.
- [26] A.-M. Pena, et al., Imaging and quantifying drug delivery in skin-Part 2: Fluorescence and vibrational spectroscopic imaging methods, Adv. Drug Deliv. Rev. 153 (2020) 147-168.
- [27] M. Egawa, Raman microscopy for skin evaluation, Analyst 146 (4) (2021) 1142-1150.
- [28] B.G. Saar, et al., Imaging drug delivery to skin with stimulated Raman scattering microscopy, Mol. Pharm. 8 (3) (2011) 969-975.
- N.A. Belsey, et al., Evaluation of drug delivery to intact and porated skin by coherent Raman scattering and fluorescence microscopies, J. Control. Release 174 (2014) 37-42.
- [30] A. Feizpour, et al., Label-free quantification of pharmacokinetics in skin with stimulated Raman scattering microscopy and deep learning, J, Invest. Dermatol. 141 (2) (2021) 395-403.
- N. Dobigeon, et al., Linear and nonlinear unmixing in hyperspectral imaging, in: Data Handling in Science and Technology, Elsevier, 2016, pp. 185-224.
- X. Xu, Z. Shi, Multi-objective based spectral unmixing for hyperspectral images, ISPRS J. Photogramm. Remote Sens. 124 (2017) 54-69.
- X. Zhang, R. Tauler, Application of multivariate curve resolution alternating least squares (MCR-ALS) to remote sensing hyperspectral imaging, Anal. Chim. Acta 762 (2013) 25-38.
- V. Olmos, et al., Relevant aspects of unmixing/resolution analysis for the interpretation of biological vibrational hyperspectral images, TrAC Trends Anal. Chem. 94 (2017) 130-140.

- [35] J.P. Smith, et al., A novel multivariate curve resolution-alternating least squares (MCR-ALS) methodology for application in hyperspectral Raman imaging analysis, Analyst 144 (18) (2019) 5425-5438.
- [36] S.J. Mazivila, J.L. Santos, A review on multivariate curve resolution applied to spectroscopic and chromatographic data acquired during the real-time monitoring of evolving multi-component processes: From process analytical chemistry (PAC) to process analytical technology (PAT), TrAC Trends Anal. Chem. (2022), 116698.
- [37] N. Feizi, et al., Recent trends in application of chemometric methods for GC-MS and GC× GC-MS-based metabolomic studies, TrAC Trends Anal. Chem. 138 (2021),
- [38] L. Liu, H. Qu, Recent advancement of chemical imaging in pharmaceutical quality control: from final product testing to industrial utilization, J. Innovative Optical Health Sci. 13 (01) (2020), 1930014.
- [39] Y.-J. Liu, et al., Data mining in Raman imaging in a cellular biological system, Comput. Struct. Biotechnol. J. 18 (2020) 2920–2930.
- W. Chen, et al., Evolution of Membrane Fouling Revealed by Label-Free Vibrational Spectroscopic Imaging, Environ. Sci. Tech. 51 (17) (2017) 9580–9587.
- [41] K. Sugiyama, et al., Raman microspectroscopy and Raman imaging reveal biomarkers specific for thoracic aortic aneurysms, Cell Reports Medicine 2 (5) (2021), 100261.
- [42] H. Rebiere, et al., Raman chemical imaging for spectroscopic screening and direct quantification of falsified drugs, J. Pharm. Biomed. Anal. 148 (2018) 316-323.
- J. Schleusener, et al., Confocal Raman imaging of skin sections containing hair follicles using classical least squares regression and multivariate curve resolution-alternating least squares, Quantum Electron. 49 (1) (2019) 6.
- [44] Choe, C.S., et al., tMCR-ALS method for the determination of water concentration profiles in the stratum corneum of untreated and treated skin in vivo. Journal of Raman Spectroscopy.
- [45] A. Stella, et al., Raman mapping coupled to self-modelling MCR-ALS analysis to estimate active cosmetic ingredient penetration profile in skin, J Biophotonics 13 (11) (2020)
- [46] A. De Juan, J. Jaumot, R. Tauler, Multivariate Curve Resolution (MCR). solving the mixture analysis problem, Anal. Methods 6 (14) (2014) 4964–4976.
- [47] H. Motegi, et al., Identification of reliable components in multivariate curve resolution-alternating least squares (MCR-ALS): a data-driven approach across metabolic processes, Sci. Rep. 5 (1) (2015) 1-12.
- C.T. Rueden, et al., Image J2: imagej for the next generation of scientific image data, BMC Bioinf. 18 (1) (2017) 1-26.
- J. Jaumot, A. de Juan, R. Tauler, MCR-ALS GUI 2.0: New features and applications, Chemom. Intel. Lab. Syst. 140 (2015) 1-12.
- [50] M.E. Wall, A. Rechtsteiner, L.M. Rocha, Singular value decomposition and principal component analysis, in: A PrActicAl ApproAch to MicroArrAy DAtA AnAlysis, Springer, 2003, pp. 91–109.
- C.W. Freudiger, et al., Label-free biomedical imaging with high sensitivity by
- stimulated Raman scattering microscopy, Science 322 (5909) (2008) 1857–1861.

 [52] Y. Yu, P.V. Ramachandran, M.C. Wang, Shedding new light on lipid functions with CARS and SRS microscopy. Biochimica et Biophysica Acta (BBA) - molecular and cell biology of, Lipids 1841 (8) (2014) 1120-1129.
- [53] Y. Li, et al., Review of stimulated Raman scattering microscopy techniques and applications in the biosciences, Advanced Biology 5 (1) (2021) 2000184.
- M.Z. Vardaki, et al., Assessment of skin deep layer biochemical profile using spatially offset raman spectroscopy, Appl. Sci. 11 (20) (2021) 9498.
- G. Pezzotti, et al., Raman spectroscopy of human skin: looking for a quantitative algorithm to reliably estimate human age, J. Biomed. Opt. 20 (6) (2015), 065008.
- M. Klaassen, E.G. De Vries, M.A. Masen, Interpersonal differences in the friction response of skin relate to FTIR measures for skin lipids and hydration, Colloids Surf. B Biointerfaces 189 (2020), 110883.
- [57] L. Wei, et al., Live-cell bioorthogonal chemical imaging: stimulated Raman scattering microscopy of vibrational probes, Acc. Chem. Res. 49 (8) (2016) 1494-1502.